AFM Nanœye – Development of an education oriented high resolution profilometer

Ioan Alexandru Ivan*, Claudie Petit*, Ion Valentin Gurgu**, Rosario Toscano*

* Université de Lyon, Ecole Nationale d'Ingénieurs de Saint-Etienne, Laboratoire de Tribologie et Dynamique des Systèmes, ENISE LTDS, CNRS UMR5513
42023 Saint-Etienne, France (e-mail: ivan@enise.fr).
** Valahia University of Targoviste, Institute of Multidisciplinary Research for Science and Technology
130004 Targoviste, Romania (e-mail: valentin.gurgu@icstm.ro).

Abstract: Currently, more and more organizations are aware of the increasing potential of nanoscience and nanotechnology, due to the wide field of innovative applications they address from biomedical and molecular technology to semiconductor and material sciences. Nanotechnology is an area where fundamental or applicative research is still in progress and where many industrial applications are waited to come. Despite the progress of this field, many institutions, notably educational ones, cannot afford investing in these technologies allowing an access to nanoscale, and a lack of knowledge therefore remains. The *Nanœye* project focuses on the widespread of Atomic Force Microscopy or AFM technology, which is the basic access tool to the nanoscale. The main goal is to design an optimal AFM model in terms of manufacturing costs by using rapid prototyping techniques and open-source hardware, and designing it as an educational-oriented equipment. This approach is two-fold: as an AFM-unexperienced user discovering its principle of operation at nanoscale or as a future engineer understanding its multi-disciplinary structure involving mechanics, optics, electronics, software and control sciences. This paper introduces the first functional structure of *Nanœye* AFM project, focusing on its mechanical structure. It is submitted to the IFAC2017 special feature Automatic Control Demonstrators.

Keywords: Atomic Force Microscope, AFM, Education, Control, Nanotechnology, Piezoelectric, Sensing

1. INTRODUCTION

Diving into the infinitely large as well as into the atomic level small has always been a source of interest, of investigation and wonder which we investigate nowadays with an ever increasing passion. Nanotechnology and Nanoscience are among those emerging fields of a dazzling ascent. Research is still starting out in various domains such as nanomedicine [Kurland], nanomaterials [Lee] or nanoelectronics, and their potential keeps appealing a crescent number of companies, because of the large innovation possibilities.

1.1 The Atomic Force Microscope (AFM)

At the nano scale we cannot draw conclusions from phenomena which intrinsically evade the direct vision. Therefore, using suitable equipment is necessary. One of the most promising yet still basic methods among the scanning probe microscopy techniques [Mironov] is the *Atomic Force Microscopy (AFM)*.

Atomic force microscopy is one of the most suitable methods to keep an eye at the nanoscale or, in other words, where our eyes are no longer able to see and to understand the origins of most phenomena related to our environment. Like the telescope for the infinitely big, the Atomic Force Microscope (AFM) is the most suitable way to access the nanoscale.

The AFM has a resolution over 1000 times better than the diffraction limit of the optical microscopes. It was the subject of a Nobel Prize in 1986 [Binnig], its structure is based on a flexible microfabricated cantilever beam with a very sharp tip, whose radius of curvature is in the range of a nanometer. The atomic-level forces which develop at close-proximity between the tip and the surface to be investigated lead to the elastic flexure of the beam, which is detected by an optical method. By raster-scanning the sample or the tip in the XY plane, a nanometer-level topography of the surface can be achieved. Several imaging modes are available, static and dynamic [Voigtlander, chap 13,14,15,17, Vancso p 25-45].

Nevertheless, despite the AFM development, such equipment still represents a high investment nowadays, notably for academic institutions, because of its prohibitive costs (over 30 k€). That is why, in spite of the wide field of promising applications it might offer, and a growing demand, this technology has a difficult spreading. Very recently the concept of low cost AFM for education [Grey] has been showing a growing interest, however the current designs (LEGO2NANO, OpenAFM, CO-AFM) still remain in early development phases. Further involvement in this direction is expected.

1.2 AFM as an education-oriented device

The AFM project called *Nanœye* aims at developing an optimized model in terms of design costs, notably thanks to *rapid prototyping techniques* [Gibson]. Moreover it was designed for an easy access and an intuitive teaching content.

The technical development aimed towards a portable prototype, which could be shown during scientific events about Microscopy or Nanotechnology. Another goal was to create a teaching kit, in the form of application notes and other documents (datasheet, user manual) necessary to learn how the equipment works and how to use it easily. The main goal is not only to design an end product, but also to encourage and support its spreading under the best circumstances, motivating and preparing the specialists and scientists of tomorrow in those promising fields of nanoscience and nanotechnology [Excoffon, Marchi].

This paper will detail the physical models on which the demonstrator is based. The second phase will present the structure of the proposed AFM model and its technical improvements towards an education-oriented instrument. Finally, some conclusions will be drawn on this first prototype on the future applicative trends of 3D-printed AFM.

2. PHYSICAL MODELLING

2.1 Interatomic potential and contact operating mode

The interactions between the AFM tip and the sample at the atomic scale result from the interatomic potential. This quantity leads to attraction when the atoms are far enough and repulsion when too close (*Fig. 1*). The repulsive force is linked to the Pauli exclusion principle preventing two electron shell structures from intersecting.
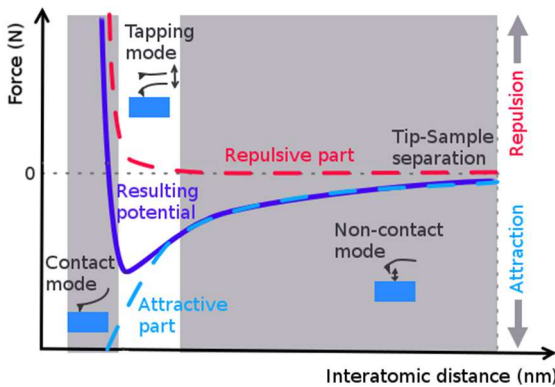

Fig. 1. Interatomic potential, its components and the different operating modes of the AFM cantilever probe

While the repulsive forces were often evaluated in an empirical way, the attractive ones result from both Van Der Waals interactions and the force interacting between static electrically charged particles, described by Coulomb's law.

The interatomic potential is a combination between attractive effects (Van Der Walls and Coulomb's law) and repulsive ones (Pauli exclusion principle). There are different empirical formulations for the global potential. One of the most well-known is Lennard-Jones potential [Voigtlander, p.147].

There are several operating modes of the AFM cantilever, namely the contact mode, tapping or oscillating mode and the non-contact mode (*Fig. 1*) [Vancso p 25-45]. In the following paragraphs will be detailed the contact mode, which was employed in this paper. The contact mode involves the repulsion forces between atoms of the tip and those of the surface of the sample because of the short working distance. When the tip is close enough to the surface while approaching the sample, it is suddenly attracted and the cantilever bends immediately down. This displacement is what we call the "snap-in" (*Fig. 2*). Once this step is acquired, the probe keeps a negative deflection when attracted by the sample. Most of the time, in contact mode, repulsive forces are involved between the tip and the sample due to the short range interaction (between the points 2 and 3 of *Fig. 2*). A control loop of the tip altitude is usually added, in order to keep a constant vertical deflection.
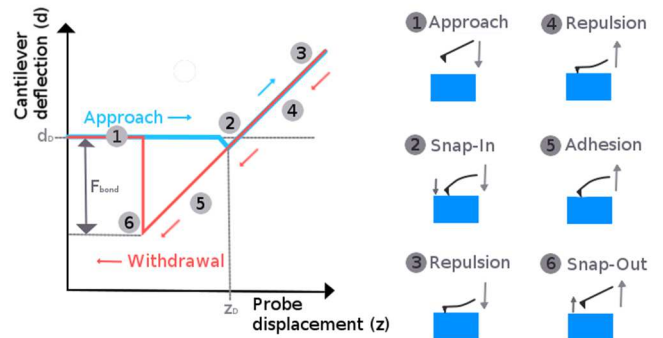

Fig. 2. Tip deflection w.r.t. the height of the cantilever base

At the end of the analysis, the tip is taken away from the surface but it tends to remain in contact due to the attraction phenomena, which result in the cantilever bending downwards. When the elastic forces finally overcome the attraction, the cantilever comes back readily to its initial state of zero deflection, which is the "snap-out" phase.

2.2 Beam theory : the end-loaded cantilever beam

The cantilever beam model has one fixed end, and thus, there is no deflection in its initial state. The end-loaded case consists in applying a load on the free end, which results in the deflection of the cantilever.
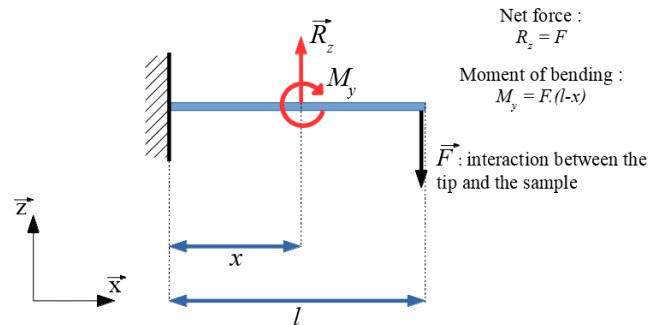

Fig. 3. The structure of the cantilever model

A simplified beam model is applied to the AFM cantilever, referring to the classical beam theory [Payam]. The cantilever is represented by its neutral axis, which links the centers of gravity of each section in the x direction (*Fig. 3*).

In this figure F represents the interaction force between the tip and the sample considering the contact mode of the AFM. The net force called Rz and the moment of bending My are related to the mechanical effects on every section of the beam. My reaches a maximum value on the fixed end, where the according distance x is equal to 0 ; in other words when $M_y = F\,l$, with l, the length. The F force involves a deflection for the cantilever as an end-load effect, according to a radius of curvature R (*Fig. 4*). The maximal vertical shifting $z(l)$ of the free end when loaded is :

$$z(l) = 4Fl^3/(Ebh^3) \qquad (1)$$

The expression (1) is valid for a cantilever with rectangular sections whose dimensions are b and h. F is applied according to the height h of the section. E is the Young's modulus.

The evolution of the deflection during the scanning is measured by an optical detection system which amplifies this very small displacement and makes it measurable. A laser spot is focused on the free end of the cantilever supporting the tip. Thus the optical beam is reflected according to the α angle, referred as between the incident beam and the normal direction (*Fig. 4*), which depends on the curvature radius R.

2.3 Optics : signal acquisition from the photosensitive sensor

As stated, a laser beam is focused on the cantilever surface. The deflection of the cantilever leads to the deviation of the reflected beam. As the distance from the tip to the detector is much larger than the cantilever length, its deflection is significantly amplified. The reflected beam is received by a photosensitive sensor : a *Position Sensitive Detector (PSD)* in this case. When the cantilever is not loaded, the non-deviated beam, R_0, reaches the active area of the sensor in an initial position which allows calibrating the optical detection system. When the probe bends during the analysis, the deviated beam is R_1 (*Fig. 4*).
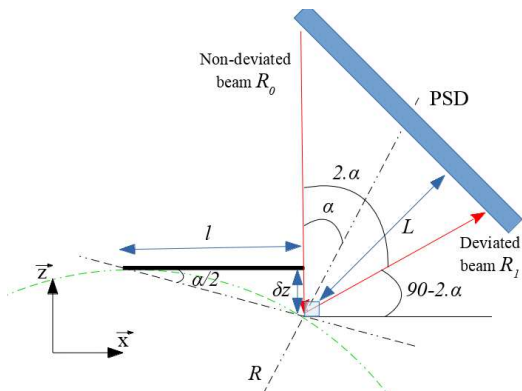

Fig. 4. General model of the reflected beam (not to scale)

The reflected beam angle depends on the length of the cantilever l and the variation of its altitude δz when it bends

(*Fig. 4*). Considering the case where the deflection and thus the angle α / 2 remain low, we obtain the following expression:

$$\tan(\alpha/2) = \delta z\,/l \approx \alpha/2 \;, \quad \alpha = 2\delta z/l \qquad (2),(3)$$
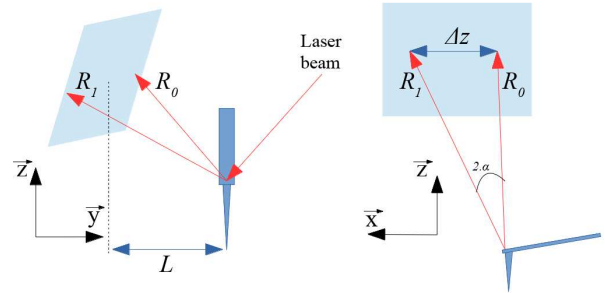

Fig. 5. Geometric configuration for the reflected beam

According to *Fig. 5*, where L is the distance between the tip and the sensor and Δz is the spot displacement, we obtain:

$$2\alpha = \Delta z/L \qquad (4)$$

From (3) and (4), we get the transfer equation:

$$\Delta z/\delta z = 4L/l = K_0 \qquad (5)$$

For the given cantilever length of 450 µm and the distance L of about 4,6 cm, the K_0 coefficient value is $K_0 = 409$.

Thus, the shifting of the measured beam on the detector is over 400 times larger than the vertical displacement of the cantilever during the analysis. For the topography metrology, this coefficient is necessary for the conversion of the measured signal into the vertical deflection of the cantilever mapping the analyzed surface. For this geometry if the PSD detection resolution is of 0.1 µm (as advertised in the datasheet) then the tip vertical resolution is of 0.25 nm.

2.4 The Position Sensitive Detector (PSD)

The *PSD* has in this case an active area to of 4x4 mm, one common cathode and four lateral anodes (*Fig. 6.*). In fact, when the active surface is exposed to a light spot, the electron flow varies towards four electrodes X_1, X_2, Y_1, and Y_2 according to the precise light spot position. In consequence, the measured currents I_1, I_2, I_3, and I_4 vary accordingly and are precisely measured by four transimpedance amplifiers.
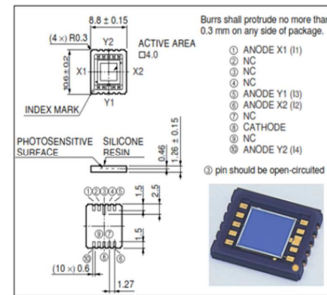
Fig. 6. Hamamatsu S5590 PSD and associated conversion equations.

2.5 Piezoelectric scanner modeling and characterization

The piezoelectric devices use the reverse piezoelectric effect, namely the deformation of a piezoelectric material upon applying an electrical field [Voigtlander, p.31-50]. The most used actuators used to build AFM scanners are the piezotubes, which allow for 3D positioning (*Fig. 7*).
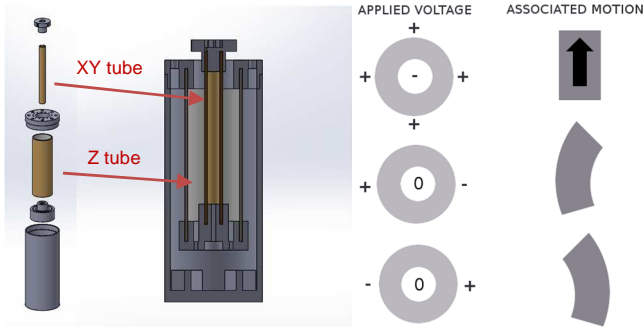

Fig. 7. Structure of the dual piezotube scanner

In the actual design there are two concentric PI Ceramic piezotubes in the scanner: the internal one model PT230.94 for the in-plane actuation (*x,y* directions) and the external one model PT230.24 for the vertical altitude actuation (*z* direction) (*Fig. 7*). Although the piezoelectric effect is nonlinear (hysteresis, creep), a linear approximation of the voltage-to-displacement characteristics by means of a proportional gain is possible, by working the basic strain-charge equations. The bending in the *xy* plane is :

$$\Delta_{x,y} = 2V_{x,y}\sqrt{2}\,d_{31}L^2 / \pi Dh \quad , \qquad (6)$$

where $\Delta_{x,y}$ is the *x* or *y* axis deflection, d_{31} is the piezoelectric transverse coefficient, *L* is the length of the tube, *D* is its outside diameter, *h* is its thickness and $V_{x,y}$ is the applied voltage used to drive the scanner in the *x* or *y* direction. The vertical actuation Δ_z, for a given voltage V_z applied across all four quadrants on the external piezotube is:

$$\Delta_z = V_z\,d_{31}\,L / h \qquad (7)$$

Some testing using a Keyence laser sensor allowed us to experimentally quantify the response of the piezoelectric scanner: the actuation gain values obtained for the three directions are resumed in *Table 1*.

Table 1. Response of the piezotube scanner

Direction	Gain (nm/V)	Total displacement* (µm)
x	108.8	21.77
y	107.1	21.43
z	21.9	4.38

*The maximal displacement corresponds to ±100V amplitude.

In fact, the response of the piezotube is highly hysteretic (*Fig. 8*) and, depending on the range of applied control signal, the slope is also non-linear, deteriorating with the increase of the applied signal voltage. For moderate voltage amplitudes such as ±20V the linear approximation (6) and (7) is quite fair.
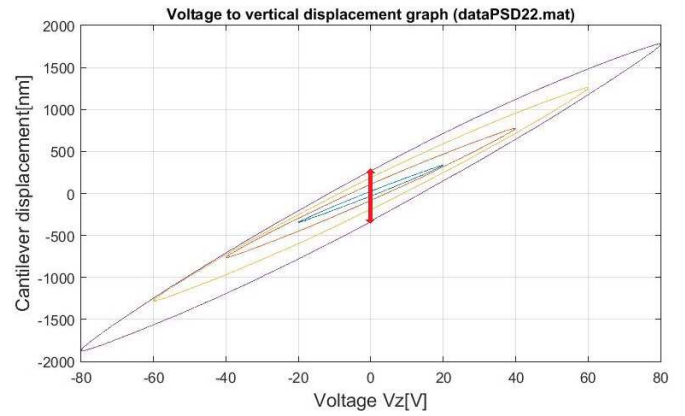

Fig. 8. Measured vertical displacement corresponding to sine waveforms of 20 V to 80 V amplitude and a slow frequency of 0.25 Hz imposed for a very accurate Keyence measurement.

3. STRUCTURE OF THE PROPOSED AFM MODEL

The main parts of the first model were printed using a stereolithography (SLA) 3D printer from Formlabs. This was an opportunity to significantly reduce the manufacturing costs without compromising the complexity of a functional model.
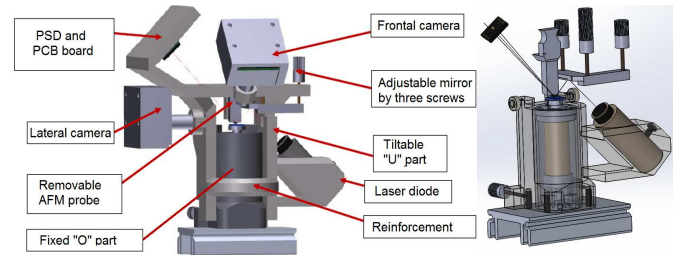

Fig. 9. CAD Model of the AFM structure and the AFM probe.

3.1 Assembly of the main parts

The AFM structure has two main parts (*Fig 10*) called "*O*" and "*U*". The *"O"* part is fixed and protects the piezoelectric scanner case. On top of the scanner platform is the sample holder which is circular. The *"U"* part supports the scanning probe, the laser and the PSD detector; it is articulated by two ball bearings for an easier access to the probe and to the mirror. A screw located on the back side of "*O*" part allows for the fine vertical positioning of the probe tip over the sample. This screw allow modifying the inclination of the *"U"* part and of the tip over the measured surface. The contact of the screw with the "*U*" part is insured by small permanent magnets. Therefore, this system also allows for close proximity approach of the sample, with a fine vertical adjustment. The AFM probe is MikroMasch HQ:CSC17

3.2 Educational-oriented design

As an equipment dedicated to teaching, the model has been conceived to make its accessible and easy to use, tweaking the common problems encountered in Scanning Probe Microscopy, such as sample view or access and manipulation of the probe.

First, the observation of the cantilever is too difficult with the naked eye, which complicates the optical adjustment and manual approach to the sample. That is the reason why the model includes cameras and adapted optical lens to get macro pictures. In order to observe both the reflected beam on the cantilever top side and its lateral deflection during the analysis, a frontal and a lateral camera are set up (*Fig. 9*). The cameras are Raspberry Pi models, chosen for their integration, cost-effectivensess and open-source features. As those camera lens did not allow macro pictures of the probe, we had to design a custom tube supporting a lens with a 10 mm focal distance.

Secondly, as the manipulation of the probe is such a delicate operation, we created a removable tip support (*Fig. 9*). This part allows the user to change the probe much more easily by simply placing it in the special window provided on the top face of the *"U"* part. In this way, positioning is both accurate and adapted to the inclination of the tip. These removable parts, each fitted with its cantilever, will be available as accessories to the microscope, which also includes a storage unit to keep them ready to use.

Some other improvements were thought like electronic design, in order to tend towards a compact shape, two electronic boards have been created: one for control signals amplification and the other for PSD signals conditioning, to convert the output signals of the sensor into the beam position measurement. These boards were integrated in the model according to the following architecture (*Fig. 10*) :
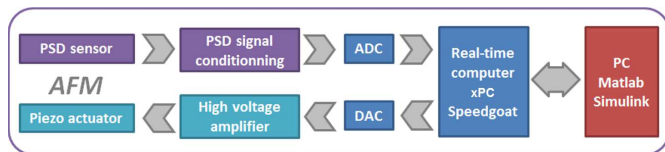

Fig. 10. Signal processing and control structure

Currently, we have built a simplified version of the external casing for the AFM unit (*Fig. 11*), which is fitted with a removable cover, used to protect the internal structure of the microscope, and isolate the PSD from the ambient light. Once removed, it provides access to the scanner, for easy observation and understanding of the AFM internal structure and also required adjustments before launching any analysis.
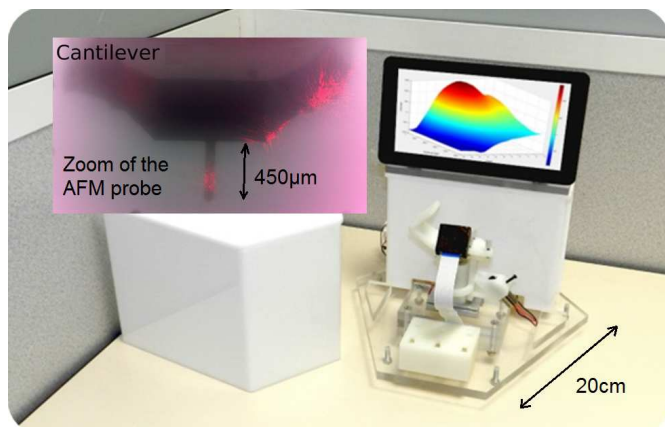

Fig. 11. Photo of the AFM prototype and macro camera view.

3.3 Control of the AFM

The Real-time computer unit (*Fig. 10*) is external, namely a xPC Speedgoat computer target running Matlab/Simulink compiled code, but we intend to accommodate in the near future a single-board computer in the rear case of *Fig. 11*.
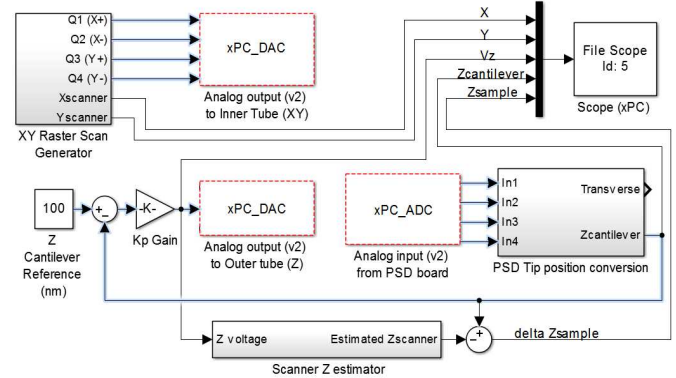

Fig. 12. Simulink control algorithm

In *Fig. 12* is detailed the Simulink model implemented in the xPC target. The scheme is quite straightforward. There is an independent open loop XY raster scan generator block based on eq. (6). The system converts the four PSD signals in the vertical δz position of the tip, according to eq. in (*Fig.6*) and (5). A simple proportional controller keeps the cantilever in contact with the probe, bended at +100 nm. The V_z applied voltage formula is thus calculated on the inversion of (7). On the same equation an estimator calculates the estimated vertical displacement of the scanner, Δ_z. This estimator is linear for the moment but in the future it will take into account the hysteretic behavior. Finally, the difference between the two vertical quantities ($\delta z - \Delta_z$) represents the vertical profile of the sample surface.

3.4 Approach-withdrawal and surface scan tests

After checking up the right functioning of the sensor and the scanner, a first series of tests consisted of bringing the tip in close contact with the sample, then sweeping up and down the scanner vertical control voltage (*Fig. 13*).
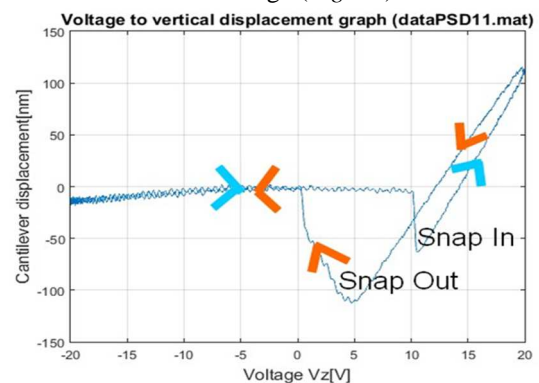

Fig. 13. AFM approach curve (amplitude ±20V, or ±438nm).

The *snap-in* and *snap-out* phenomena readily appear on the PSD output readings, which corresponds to the bonding and detachment of the tip to the sample respectively, due to the

local atomic interaction. The two curves are slightly separated due to the piezoelectric hysteretic behavior.

The noise level expressed in terms of RMS (root mean square) values is quite good for this prototype, in the nanometer range. The RMS value is of 1.1 nm for the out-of-contact condition and 0.7 nm for the in-contact state.
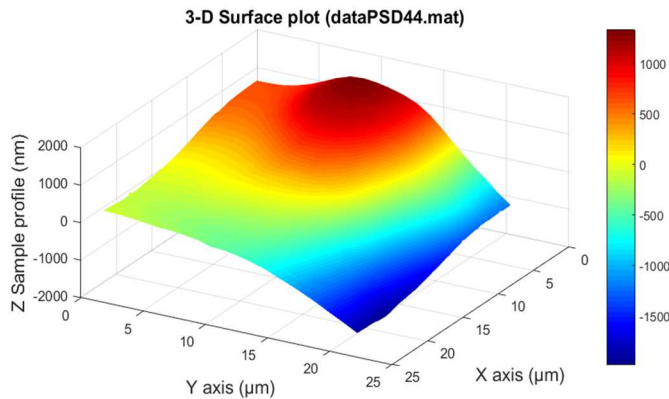

Fig. 14. Image of a NdFeB magnet (22 lines by 2000 points, scan rate 2 seconds per line, z-control sampling period 0.1ms).

The second type of tests consisted of actuating the piezotube with the attached sample in a raster scan mode, line after line, over the whole analyzed area and with a vertical control according to Section 3.3. The acquired data on each measurement point was recorded and transposed to a color scale and a 3D graph of the profile (*Fig. 14*). This image successfully demonstrates the AFM, however the main disadvantage of working in *"Force" contact mode* is that the tip cannot follow profile variations too steep, and it gets out of contact when the sample presents large rugosity, as in the case of our first scan trials.

4. CONCLUSION

This educational AFM project is multidisciplinary (mechanics, optics, electronics, control systems, software) and touches several booming fields such as *nanotechnology, additive manufacturing* or *embedded electronics*. It has been dedicated to undergraduate students in mechanical engineering but can be adapted from high school to post graduated. The low cot 3D-printed AFM is quite a novel concept in the field, which clearly presents the advantages of reduced manufacturing and design costs, all without compromising reliable *nanometer resolution*. The overall weight of the system is thus reduced (portable AFM). Other notable advantage for education is in AFM internal structure, which is visible and documented.

The first proof of concept of the *Nanæye* project using a linear model and open-loop controller has been presented and experimentally validated, showing performance similar with other equivalent entry-level equipment. The internal structure and some tests have been highlighted. The linear approximation worked well for driving voltages below ±20V.

The work is still in progress, namely for a further improved and more robust design of the "*U*" part, for the addition of the "tapping" operation mode and for the integration of an embedded computer and a more intuitive human-computer interface. The piezotubes are highly nonlinear in and the open loop operation leads to in-plane distortion. Adding capacitive sensors highly increases the costs. We intend to replace the piezotubes by voice-coils, which are linear and cost-effective.

Hopefully, *Nanæye* project will achieve a functional and affordable equipment, enabling an easier dissemination of the AFM and nanotechnology towards the engineers and scientists of tomorrow.

REFERENCES

Binnig, G., Quate, C.F., and Gerber, C. (1986). Atomic force microscope. *Physical Review Letters*, 56, 930-933.

Excoffon, E., Papillon, F., Fresquet, L., Bsiesy, A., and Bonnaud, O. (2012). New pedagogical experiment leading to awareness in nanosciences and nanotechnologies for young generations at secondary school. *Information Technology Based Higher Education and Training (ITHET), 2012 International Conference on, IEEE Xplore.*

Grey, F., (2015). Creativity unleashed, *Nature Nanotechnology* 10, 480

Gibson, I., Rosen, D.W., and Stucker, B., (2010). *Additive manufacturing technologies,* Springer, New York (USA).

Kurland, N.E., Drira, Z., and Yadavalli, V.K., (2012). Measurement of nanomechanical properties of biomolecules using atomic force microscopy. *Micron*, 43, 116-128.

Lee, S.W., (2016). Mechanical properties of suspended individual carbon nanotube studied by atomic force microscope. *Synthetic Metals*, 216, 88-92.

Marchi, F., Castet, J., Marlière, S., Castagné, N., Chevrier, J., Luciani, A., and Florens, J.L., (2010). Le concept du NanoLearner : les mains dans le Nanomonde du grand pu- blic à l'université. *Proceedings of 8ème Colloque sur l'enseignement des Technologies et des Sciences de l'Information et des Systèmes.*

Mironov, V.L. (2004). *Fundamentals of scanning probe microscopy*, 98, The Russian Academy of Sciences Institute for Physics of Microstructures, Nizhniy Novgorod (Russia).

Payam, A.F., Fathipour, M., (2009). Modeling and dynamic analysis of atomic force microscope based on Euler-Bernoulli beam theory. *Digest Journal of Nanomaterials and Biostructures*, 4, 565-578.

Vancso, G.J., Schonherr, H., (2010*). Scanning Force Microscopy of polymers*, 3-73, Springer, Berlin (Germany).

Voigtlander, B., (2015). *Scanning Probe Microscopy : Atomic Force Microscopy and Scanning Tunneling Microscopy*, 31-50, 145-275, Springer, New York (USA).